Geophysical Journal International

Geophys. J. Int. (2016) **205,** 1032–1048
Advance Access publication 2016 February 8
GJI Marine geosciences and applied geophysics

doi: 10.1093/gji/ggw051

Exploration of resistive targets within shallow marine environments using the circular electrical dipole and the differential electrical dipole methods: a time-domain modelling study

Amir Haroon,[1] Vladimir Mogilatov,[2] Mark Goldman,[3] Rainer Bergers[1] and Bülent Tezkan[1]

[1]*Institute of Geophysics and Meteorology, University of Cologne, D-*50923 *Cologne, Germany. E-mail: haroon@geo.uni-koeln.de*
[2]*Novosibirsk State University,* 630090 *Novosibirsk, Russia*
[3]*Department of Marine Geosciences, University of Haifa,* 3498838 *Haifa, Israel*

Accepted 2016 February 1. Received 2016 February 1; in original form 2015 April 2

SUMMARY

Two novel transient controlled source electromagnetic methods called circular electrical dipole (CED) and differential electrical dipole (DED) are theoretically analysed for applications in shallow marine environments. 1-D and 3-D time-domain modelling studies are used to investigate the detectability and applicability of the methods when investigating resistive layers/targets representing hydrocarbon-saturated formations. The results are compared to the conventional time-domain horizontal electrical dipole (HED) and vertical electrical dipole (VED) sources. The applied theoretical modelling studies demonstrate that CED and DED have higher signal detectability towards resistive targets compared to TD-CSEM, but demonstrate significantly poorer signal amplitudes. Future CED/DED applications will have to solve this issue prior to measuring. Furthermore, the two novel methods have very similar detectability characteristics towards 3-D resistive targets embedded in marine sediments as VED while being less susceptible towards non-verticality. Due to the complex transmitter design of CED/DED the systems are prone to geometrical errors. Modelling studies show that even small transmitter inaccuracies have strong effects on the signal characteristics of CED making an actual marine application difficult at the present time. In contrast, the DED signal is less affected by geometrical errors in comparison to CED and may therefore be more adequate for marine applications.

Key words: Electromagnetic theory; Non-linear electromagnetics; Marine electromagnetics.

1 INTRODUCTION

Until present, many marine controlled source electromagnetic (CSEM) applications focus on detecting resistive bodies, that is, hydrocarbon (HC) saturated reservoirs embedded in a conductive background environment (e.g. Eidesmo *et al.* 2002). The most general application utilizes a horizontal electrical dipole (HED) transmitter exciting a continuous, low-frequency waveform along with multiple inline electromagnetic (EM) receivers. This method, commonly referred to as the frequency-domain controlled source electromagnetic (FD-CSEM or just CSEM) method, shows exceptional signal detectability towards resistive targets and, compared to other well-established land-based EM methods, is quite practical to apply within the marine environment. As a result, several academic and industrial institutions have developed their own FD-CSEM systems generally consisting of a towed transmitter dipole accompanied by several seafloor-based receivers (e.g. Chave *et al.* 1991; Constable 2010).

One drawback of the FD-CSEM system is the influence of the insulating air half-space on the measured signal that becomes especially prominent in shallow-sea applications. For FD-CSEM measurements in shallow water, the signature of the air–sea interface may dominate the signal at large offsets and, as a result, sensitivity towards the subseafloor resistivity structure will be limited (Connell & Key 2013). Under these circumstances, the measured signal typically decays by $1/r^3$ at large offsets, where r represents the distance between transmitter and receiver. This geometrical decay is attributed to the effect of the so-called airwave (Weidelt 2007).

As an alternative, several marine CSEM applications are considered in the transient mode (time-domain or TD) where the 'shallow-water problem' is less severe in terms of masking the resistive target (Weiss 2007; Chen & Alumbaugh 2011). Furthermore, methods exciting EM fields that are independent of the airwave signal have received an increased attention in scientific literature. The most popular in terms of recent practical and theoretical developments being the vertical electrical dipole (VED), also

called vertical electrical lines (VEL; e.g. Scholl & Edwards 2007; Holten *et al.* 2009; Helwig *et al.* 2013; Singer & Atramonova 2013; Barsukov & Fainberg 2014). In a 1-D setting, the EM field of the latter is solely described by a unimodal transverse magnetic (TM) field meaning the absence of vertical magnetic fields and presence of a vertical electric field. As a result, the excited TM field leads to an increased target response towards resistive layers in comparison to unimodal transverse electric (TE) field methods. Despite this characteristic, the drawback of applying unimodal TM-mode methods is the smaller signal amplitude (Chave & Cox 1982). However, the unimodal TM field is not crucially influenced by the airwave and, therefore, predestined for shallow-sea applications. And although VED is considered a unimodal TM-mode method, its applicability in shallow sea is quite troublesome. On the one hand, the depth of the water column restricts the extent of the transmitter antenna. Hence, the limited dipole moment may result in a poor signal-to-noise ratio (SNR). On the other hand, the method suffers from the severe non-verticality effect (e.g. Goldman *et al.* 2015) that makes its application in shallow water rather problematic.

As an alternative to VED, we theoretically substantiate a further unimodal TM-mode method called circular electrical dipole (CED). This transmitter system was originally designed for land measurements as a surface-based equivalent of the VED, to avoid the use of boreholes (Mogilatov 1992, 1996). As stated above, the application of VED in a shallow-sea environment is associated with several issues. Consequently, Goldman *et al.* (2015) suggest a CED application within shallow marine environments to benefit from the advantages of using unimodal TM-mode methods and avoid the use of VED's.

Additionally, the application of a completely novel marine EM method called differential electrical dipole (DED) is proposed. The transmitter consists of two electrical dipoles in an inline configuration with a common central electrode. The central electrode has one polarity, whereas the two outer electrodes have the other polarity. A similar idea of using differentially normalized electromagnetic method (DNME) is discussed in Russian literature (e.g. Legeydo *et al.* 1990, 1997). The method works by injecting the current through an electrical dipole and the electrical receivers are used to create the differential signal. The DED approach suggests producing the differential signal through the application of a double-dipole transmitter system.

In the course of this study, we will compare DED and CED to the conventional time-domain CSEM and VED methods. The theoretical basis of the former methods is described and rigorous 1-D and 3-D modelling is used to study resistive targets within a conductive background environment. Furthermore, signal distortions caused by asymmetry of the complex transmitter geometry are studied and elaborately discussed in terms of applicability.

2 METHODS

This study focuses on the comparison of four time-domain EM methods. The theory of an HED field excitation in a 1-D subsurface can be found in numerous publications (e.g. Edwards 2005). For a VED source, refer to Scholl & Edwards (2007) and for loop sources to Swidinsky *et al.* (2012). In contrast to HED, VED and even loop sources, CED and DED are rather unfamiliar and will be elaborately discussed. Both methods have their origin in Russia and were originally developed for land-based hydrocarbon investigations. A joint application was recently performed in Russia.

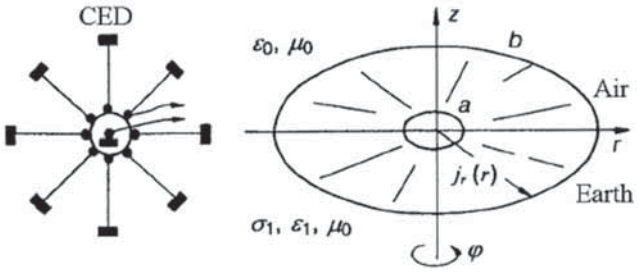

Figure 1. Sketch of an approximated CED transmitter on the left and an idealized CED transmitter with an inner radius of a and an outer radius of b on the right (Mogilatov & Balashov 1996).

2.1 Marine circular electrical dipole

The advantages and disadvantages of time-domain VED systems have been discussed in preceding literature (e.g. Goldman *et al.* 2015). On land, an analogue EM field of the VED can be realized by applying a surface-based CED. This idea was first introduced by Mogilatov (1992) and practically realized by Mogilatov & Balashov (1996) for two main reasons: (1) To avoid the necessity of boreholes during the measurement that are often time and cost consuming and (2) to circumvent the issue of perfect verticality by VED measurements that can be problematic even in predefined boreholes.

As shown in Fig. 1, the ideal CED transmitter consists of a continuum of 'outer electrodes' arranged in a circle around a central electrode. In practice, Mogilatov & Balashov (1996) show that an ideal CED transmitter is sufficiently approximated by using eight outer electrodes with one polarity arranged in a circle around the mutual, central electrode with the other polarity. The current between the inner and outer electrodes flows through insulated wires.

One of the major shortcomings of CED is the strict criterion of equal current amplitudes in the eight electrical dipoles. This task may be quite cumbersome for land-based measurements due to different coupling conditions of the outer electrodes. This issue has been successfully solved through the development of a transmitter system that regulates the current in the eight arms individually (Helwig *et al.* 2010). Within the marine environment, the coupling problem is expected to be less severe due to the homogenous surroundings (sea water). The issue of maintaining equal currents is expected to be less challenging.

When assuming a 1-D subsurface, the EM field of a CED is described by a unimodal TM field, irrespective of the z-location of the transmitter. The radial EM field of a CED transmitter situated at any interface of a layered earth model is described by the following Hankel transform,

$$E_r(r) = \frac{I_0 b^2}{8\pi} \int_0^\infty J_1(kr) \cdot k^2 \frac{P_1 Q_1}{P_1 + Q_1} dk \qquad (1)$$

where I_0 is the current amplitude, J_1 is the first kind Bessel function of order 1, b is the radius of the CED transmitter, Q_1 and P_1 are the transfer functions just below/above the source layer and k is the wavenumber. The complete derivation of eq. (1) is given in the Appendix. The Hankel transform in eq. (1) can be evaluated in the time domain by using appropriate digital filter techniques as described by Johansen & Sørensen (1979).

Similar to VED, CED is a zero-field method meaning that a magnetic field is absent over a stratified 1-D subsurface. Previous land-based field measurements successfully exploited this characteristic by using CED as a mapping tool for resistive 3-D bodies embedded

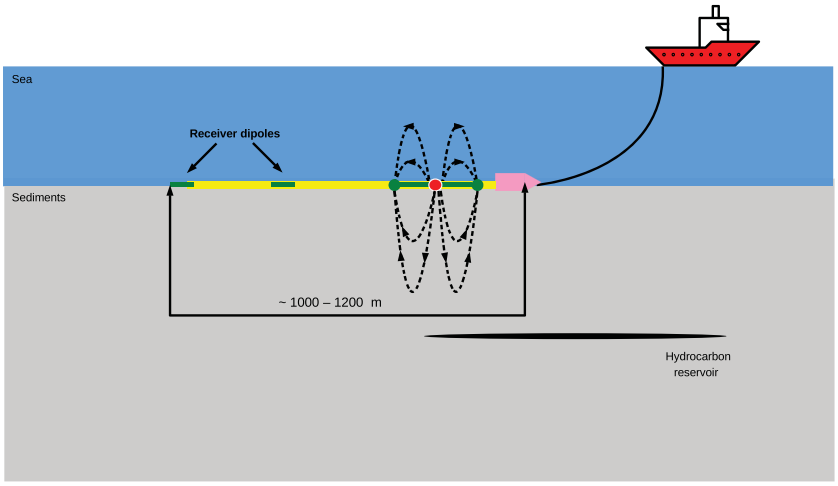

Figure 2. Schematic sketch of a DED system in a marine setting. The transmitter consists of two opposite dipoles in an inline configuration. The dashed lines display the excited current system in the *xz*-plane.

in predominantly 1-D background environments. The 3-D boundaries of hydrocarbon reservoirs were successfully mapped using a large, fixed CED transmitter of several hundred metre radii accompanied by mobile, magnetic field receivers (Mogilatov & Balashov 1996; Helwig *et al.* 2010).

Although this feature is unique for mapping resistive 3-D targets, the application of large CED transmitters is hardly feasible in marine applications. Therefore, the theoretical considerations of a marine CED application, previously shown by Goldman *et al.* (2015), suggest using the CED as a short-offset sounding method. The suggested system confines to transmitters of several tens to one hundred metres radii with short-offset electric field receivers (2–5 CED radii distance). This restriction will primarily lead to poor SNR due to the limited extent of the CED antenna in comparison to the conventional TD-CSEM systems. Yet, the following study will theoretically assess CED signals in both short- and long-offset configurations while keeping the poor SNR in mind as the limiting factor for future CED applications.

2.2 Marine differential electrical dipole

The application of a marine DED system is, to our knowledge, a novel approach. A similar approach called DNME has indeed been presented in Russian literature (Bubnov *et al.* 1984; Legeydo *et al.* 1990, 1997; Mandelbaum *et al.* 2002). The difference to DED is that the DNME system applies a normal HED transmitter to inject the current while the differential signal is obtained through the receiver geometry. For the proposed DED system, the current is injected differentially through a three-electrode transmitter. Theoretically, Davydycheva & Rykhlinski (2011) discussed the application of a focused-source EM (FSEM) method that essentially is identical to the application of DED (as suggested incomplete axial focusing mode). They use 3-D modelling studies to demonstrate the improvement of FSEM compared to both FD-CSEM and TD-CSEM. Veeken *et al.* (2009) successfully applied a DNME system in marine hydrocarbon exploration. Also, some land-based DED measurements (generally referred to as counter lines) have been performed in conjunction with CED.

As illustrated in Fig. 2, the DED transmitter consists of a double-dipole system, where the two HED's share a common central electrode. The current in each dipole flows in opposite directions. Unlike CED/VED, a DED transmitter excites a bimodal EM field consisting of both TE and TM mode. The sensitivity towards resistive layers embedded in a conductive background is, therefore, similar to TD-CSEM.

Contrary to all other methods subjected in this study, DED has not been extensively discussed in terms of detectability towards resistive targets in a shallow marine setting. In the course of this study, we compare DED signals to TD-CSEM, CED and VED for both, short and long offsets. The aim is to assess the detectability characteristics and lateral resolution in comparison to CED, VED and TD-CSEM.

3 ONE-DIMENSIONAL FORWARD MODELLING

The aim of the 1-D modelling studies is to demonstrate the signal detectability of the investigated EM methods toward resistive target layers, for example, HC-saturated layers embedded in conductive background environments. The main focus is the shallow water environment (water column has a maximum thickness of 100 m). We do not attempt to present a feasible marine system of any particular configuration (transmitter length, offset, etc.), but rather to give a fair comparison between the time-domain methods CED, DED, TD-CSEM and VED. Therefore, all investigations will be presented for both short- and long-offset configurations. It should be noted that the short-offset configuration clearly favours the CED/VED systems, whereas the long offset is best applied for TD-CSEM measurements. Unless stated else, all 1-D modelling studies were performed using 100 m dipoles with 1 A current.[1]

To compare the signal detectability of resistive targets for different EM methods, a simple three-layer resistivity model is used (see Fig. 3). A resistive target layer of variable thickness and 100 Ωm resistivity is embedded in marine sediments (1 Ωm) at a depth of 1000 m beneath the seafloor. The thickness of the target layer varies between values of 10, 50, 100, 200, 500 and 1000 m. The water column has a thickness of 100 m and a resistivity of 0.333 Ωm. Offsets of 400 and 5000 m were chosen corresponding to a short- and long-offset configuration, respectively. For CSEM, CED and

[1] Dipole lengths are meant. The TD-CSEM/VED is, therefore, 100 m long whereas CED/DED has a radius of 100 m.

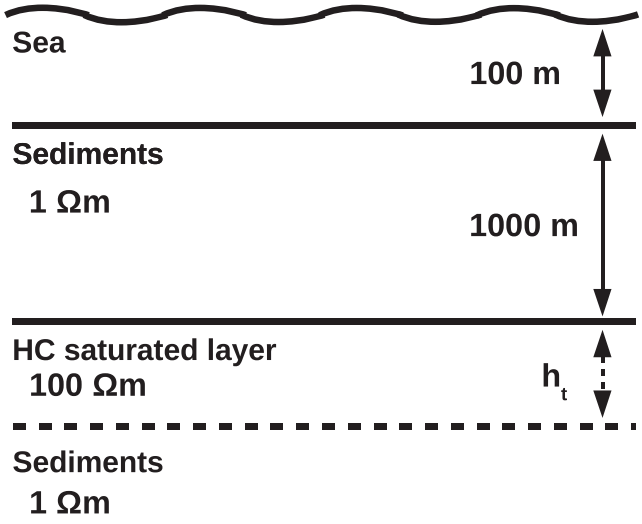

Figure 3. Layered earth model representing a hydrocarbon (HC) saturated layer embedded in marine sediments. The thickness (h_t) of the resistive HC layer is varied between 10 and 1000 m.

DED, both transmitter and E_r receiver are located on the seafloor. For VED, the vertical transmitter fills the complete water column with an E_r receiver located on the seafloor.

The calculated step-off forward responses are presented as transients in the left column of Figs 4 and 5. Additionally, the same transients are displayed as curves normalized to a 1 Ωm host half-space (no target) in the right column. This very basic characteristic serves as a tool to interpret the response of the resistive layer on the calculated data while neglecting other aspects of EM measurements, that is, SNR, equivalence, etc. that may become relevant when interpreting actual data.

In Fig. 4, the 1-D forward response of CSEM, VED, DED and CED is shown for a short-offset configuration ($r = 400$ m). The superior detectability of CED/VED is clearly notable in comparison to both TD-CSEM and DED. However, since the TD-CSEM signal is known to be sensitive towards resistors only at large offsets, this comparison is rather biased. Nonetheless, CED and VED signals can detect very thin resistive layers of 10 m thickness at a depth of 1000 m beneath the seafloor. In comparison, the normalized response of TD-CSEM at short offsets shows little to no response towards very thin resistive layers (10 m thickness). As mentioned, this is primarily due to the short-offset configuration applied in this study. Layer thicknesses of 50 m are distinguishable from the half-space response in the DED signals, whereas TD-CSEM still lacks the necessary detectability. For thickness of 100 m or greater, all methods show a significant response towards the resistive layer. Yet, a clear distinction of signals between different resistor thicknesses may be quite ambitious when analysing the TD-CSEM response.

One characteristic that should not be neglected is the signal amplitude and dynamics that become relevant issues in field measurements. In respects to the former, TD-CSEM clearly dominates all other methods by 4–5 orders of magnitude at late times. In noisy background environments, this may be the logical inference of choosing TD-CSEM above any other method. However, successful VED applications have been performed using current amplitudes of up to 6000 A to obtain the necessary SNR (Helwig *et al.* 2013). Therefore, the superior detectability of CED, VED and DED may justify future applications, as signal strength is more of a technical issue that becomes less severe as technology develops.

In the long-offset configuration ($r = 5000$ m) shown in Fig. 5, the situation is somewhat different. All methods, including TD-CSEM show a measureable detectability towards very thin resistive targets. This is mainly due to the strong effect of the resistive layer on the DC-level that is represented in the very early times of the transient. However, when analysing the transient decay, CED/VED still show a stronger response towards the resistive layer. Again, DED seems to have enhanced detectability characteristics in comparison to TD-CSEM. In terms of signal amplitude and dynamics, the situation is similar in comparison to the short-offset configuration. The amplitudes of TD-CSEM are two orders of magnitude larger compared to the other methods.

It is safe to say that CED/VED exhibit a sufficient target response in the short- and long-offset range, even for very thin resistive layers. Whether this characteristic may be exploited in actual field measurements remains to be determined due to the very small signal amplitudes. This issue and the resulting SNR have to be considered before attempting actual measurements. TD-CSEM transients have large signal strengths but a much lower target response. DED is somewhere in between CED/VED and TD-CSEM in terms of detectability and signal strength. This particularly applies to short-offset range where DED shows a sufficient target response in comparison to TD-CSEM, which exhibits practically no response towards the resistive layer. However, in comparison, the latter has advantages due to the larger signal amplitudes.

4 THREE-DIMENSIONAL FORWARD MODELLING

A 3-D modelling study is performed to compare CED, DED, TD-CSEM and VED responses to a finite resistive slab of 100 Ωm and a thickness of 100 m. Such model more adequately represents real HC-saturated reservoirs than the above considered 1-D earth. As displayed in Fig. 6, the lateral extent of the slab is considered to be either 900 m × 900 m or 4500 m × 4500 m shown by red and blue blocks, respectively. The former representing a resistive body with dimensions smaller than the depth of burial and the latter one that is much larger. The sea water layer is assumed to have a perfectly lateral bathymetry with a thickness of 100 m. The profile curves displayed in Fig. 7 show time delays (dt) calculated for each method and plotted against the transmitter position (in kilometres) along a profile crossing directly above the resistive body. Since the 1-D modelling studies show that TD-CSEM is sensitive towards the resistor at early times whereas the other three methods at late times, different time delays were chosen. A time delay of 0.45 s was chosen for TD-CSEM complying with the time range of high detectability of the 1-D modelling. For CED, VED and DED a time delay of 10 s was chosen. Generally, the profile curves of the latter three methods show comparable behaviour at sufficiently late times. The time delay of $dt = 10$ s was therefore chosen arbitrarily. It should be mentioned that a comparison of signal strengths between TD-CSEM and the other methods would be rather biased toward TD-CSEM at this point, as amplitudes will be stronger at early times for a step-off current excitation. Hence, the chosen time delays would favour the TD-CSEM signals in terms of signal amplitudes. Yet, if the SNR would be the only factor of consideration, TD-CSEM is clearly superior to the other methods.

The centre of the resistive body is located at 0 m. Again, both short- and long-offset configurations are investigated with receivers Rx1 and Rx2, respectively. Similar offsets to the 1-D modelling

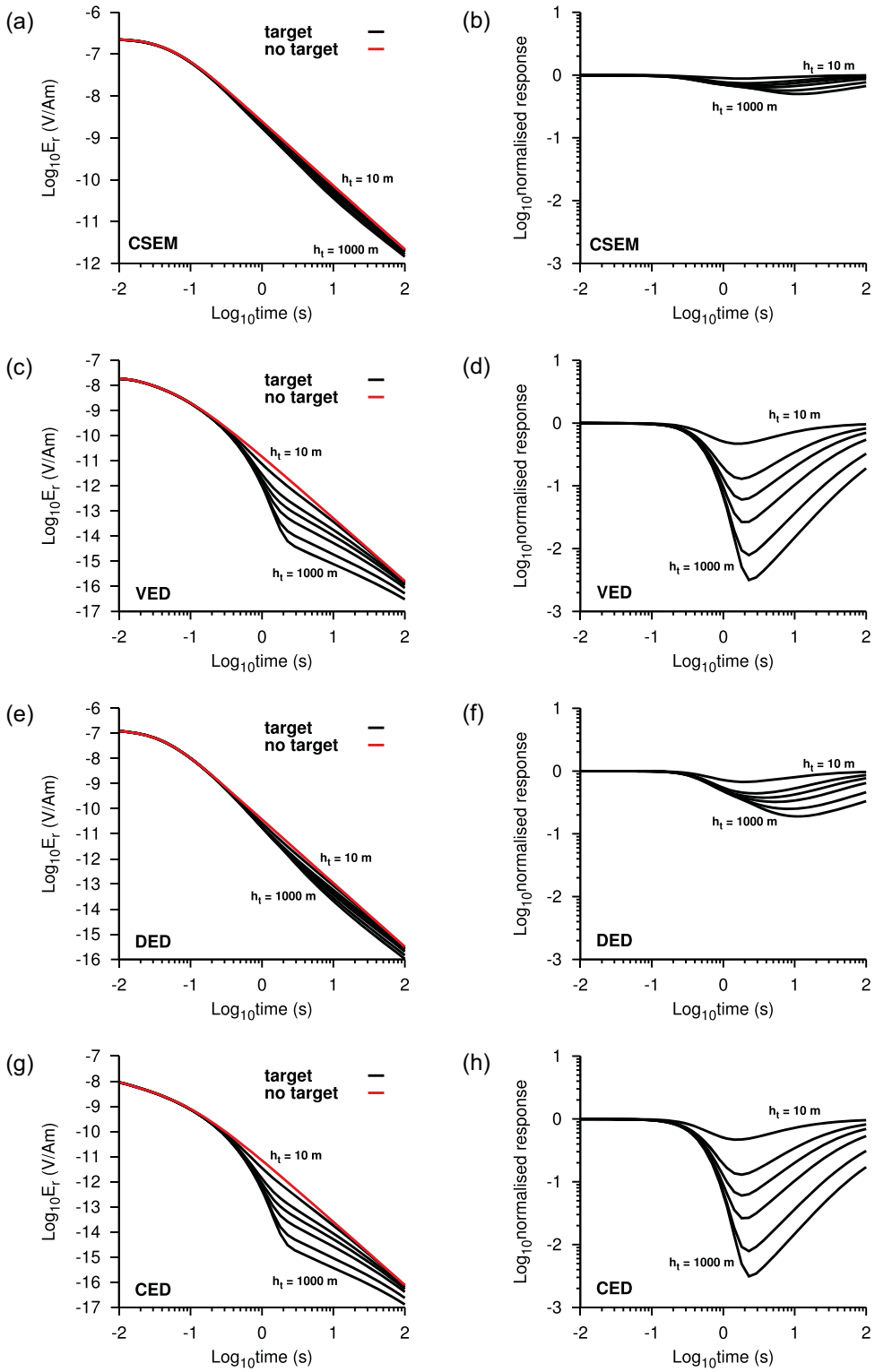

Figure 4. Results of 1-D modelling study shown in Fig. 3 for a short-offset configuration ($r = 400$ m). The step-off transients of CSEM, VED, DED and CED are displayed in (a), (c), (e) and (g), respectively. The transients of the left column are also displayed as normalized responses (ratio of target to no target) for all methods in the right column for better representation of detectability.

study were chosen. The minor differences are due to the grid design of the finite difference modelling code. All 3-D modelling studies are performed with the finite-difference software SLDMEM3t based on a modified spectral Lanczos decomposition method first introduced by Druskin & Knizhnerman (1988, 1994).

Goldman *et al.* (2015) presented a similar 3-D modelling study focusing on the lateral resolution of CED and VED in a short-offset configuration for water depths of 100 and 1000 m. They argue that both VED and CED have exceptional lateral resolution capabilities in comparison to the FD-CSEM method, even in deep-sea

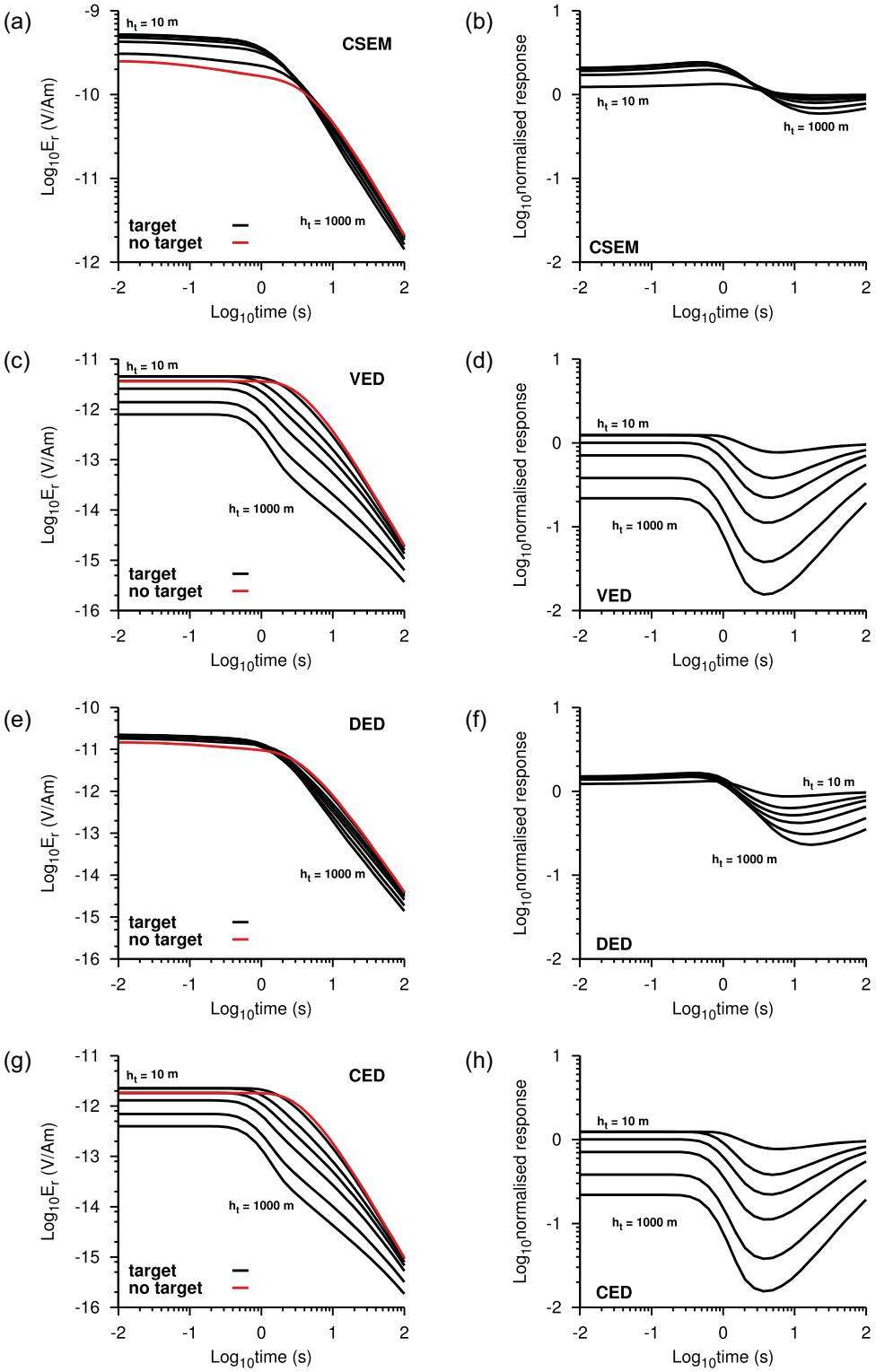

Figure 5. Results of 1-D modelling study shown in Fig. 3 for a long-offset configuration ($r = 5000$ m). The step-off transients of CSEM, VED, DED and CED are displayed in (a), (c), (e) and (g), respectively. The transients of the left column are also displayed as normalized responses (ratio of target to no target) for all methods in the right column for better representation of detectability.

environments. CED/VED shows a considerable response towards small resistive bodies with lateral dimensions smaller than the depth of burial. In the short-offset configuration, the signals of CED and VED remarkably follow the shape of the resistive body. Furthermore, they state that for shallow marine applications CED is even more effective in comparison to VED since the depth of the water column does not limit the dipole moment and an SNR issue is less likely.

Whereas Goldman *et al.* (2015) used a VED-E_z receiver configuration as it is applied commercially (i.e. Helwig *et al.* 2013), this

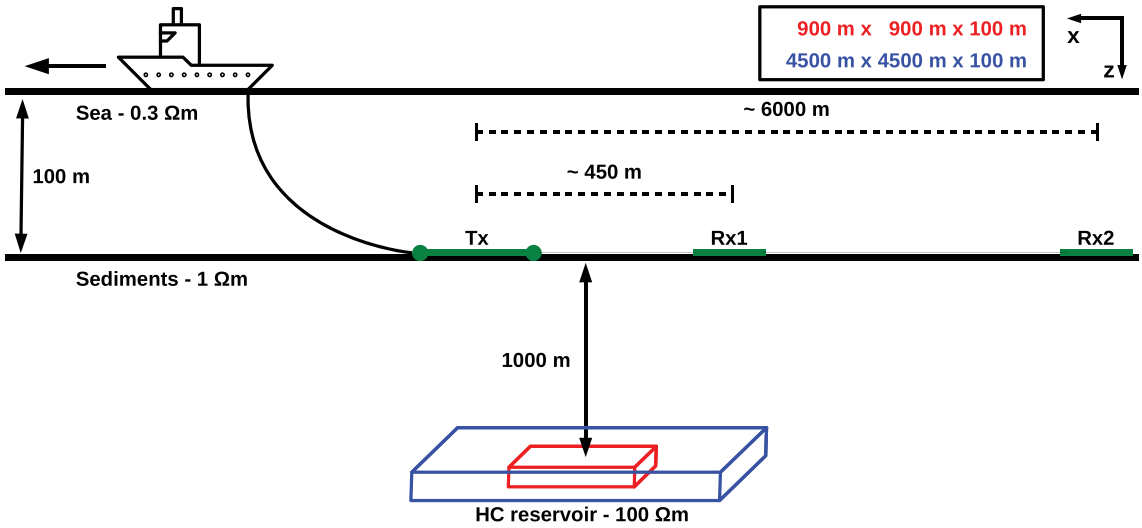

Figure 6. 3-D modelling study representing a HC-saturated body with a resistivity of 100 Ωm and a thickness of 100 m is embedded in marine sediments. The lateral dimensions of the resistive body are finite with either 900 m × 900 m or 4500 m × 4500 m. The four EM systems are towed over the centre of the body with receiver offsets of approximately 450 and 6000 m representing the short- and long-offset acquisition.

modelling study confines to E_r-receivers. Compared to Goldman *et al.* (2015), the offset between Tx and Rx1 in the short-offset configuration is of a factor 2–4 times larger. Nonetheless, the general results of Goldman *et al.* (2015) for short offsets are reproducible. The signal follows the shape of the resistive body with amplitude maxima directly over the edge of the body. Furthermore, the signals of CED and VED are practically identical although amplitudes differ by a half order of magnitude. If SNR is neglected in the theoretical assessment, the study shows that CED and/or VED assuming a conductive homogeneous host medium may easily detect resistive bodies with rather small lateral dimensions and thicknesses of 100 m or more. Moreover, the lateral boundaries of the resistive body are easily pinpointed using both methods as the signal amplitudes are at a maximum.

The signal amplitudes of TD-CSEM are approximately 4–5 orders of magnitude larger compared to the other methods (Fig. 7a). This large difference in signal amplitude is partly explained by the chosen time delays of the profile curves but also reflects the advantages of TD-CSEM applications. However, the signal shows no significant response towards the resistive 3-D bodies at short offsets, which again is attributed to the chosen (short-offset) configuration. For a larger 3-D reservoir, small deviations from the background signal are notable. However, if this signature can be measured is debateable. Hence, for geological targets of this kind, an application of short-offset TD-CSEM is not advisable. In contrast to TD-CSEM, the profile curves of DED (Fig. 7e) are very similar to CED/VED. This contradicts the 1-D modelling results where the detectability of DED was only slightly better compared to TD-CSEM. The DED signal follows the shape of the resistive body and is, therefore, in unison with the signals of CED/VED. Depending on the drag direction, the signal may reach either maximum, or minimum amplitude above the reservoir edges. This may be considered a disadvantage compared to CED/VED where the amplitudes are at maximum compared to the 1-D background. Thus, the SNR level may become a relevant issue over one of the reservoir boundaries when applying DED. However, the DED signal of background half-space exceeds those of CED/VED by almost one order of magnitude and may, therefore, be considered more suitable in terms of SNR.

The situation slightly changes in a long-offset configuration (Fig. 7, right column). The most obvious change is that the signal dynamics of all methods is decreased in comparison to the short-offset configuration. The amplitude of TD-CSEM now exceeds the other methods by 2–3 orders of magnitude. In the long-offset configuration, all methods are rather insensitive towards the small resistive body. However CED and VED signals still show a significant response. The DED signal displayed by the red line in Fig. 7(f) shows a response towards the small resistive body, but may generally be too small to be distinguished from the background. In comparison, the TD-CSEM signal shows practically no response towards the 900 m × 900 m reservoir.

In comparison to the small resistive target (red line), the large resistive body is detected by all methods at large offsets. The TD-CSEM response is approximately a factor 2 larger compared to the background response. This is attributed to the DC contribution of the signal, which would be characterized by higher absolute amplitudes if a resistive body was present in the subsurface. In comparison, CED, VED and DED all show a decrease in signal amplitudes for a resistive 3-D body. The signals are generally of a factor 2–3 smaller compared to the background. In comparison, the signal of the latter three methods follows the shape of the reservoir, whereas the signal of CSEM deviates from the background only if either transmitter or receiver is located over the reservoir. Therefore, the profile curves of CSEM are off-centre. In comparison to the short-offset configuration, CED, VED and DED do not resolve the shape of the aquifer as accurately. Yet, a distinction of the lateral boundaries would seem feasible using these profile curves. As mentioned, the signal of TD-CSEM indeed possesses a measurable signature of the reservoir if either transmitter or receiver (located at −6 km from the transmitter) is located directly above it. However, the signal does not give a clear distinction of the lateral boundaries as for the other three methods. Therefore, the delineation of the lateral boundaries would seem easier to interpret when applying CED, VED or DED. Yet, as the signal amplitudes of the latter methods are minimal above the centre of the body, an SNR issue may become relevant for these applications.

The clear advantage of TD-CSEM compared to the other methods is the signal amplitude; both in the short- and long-offset setting. However, TD-CSEM has a limited response to a resistive block with finite dimensions, especially if compared to the other methods. In turn, CED, VED and DED may seem superior in terms of

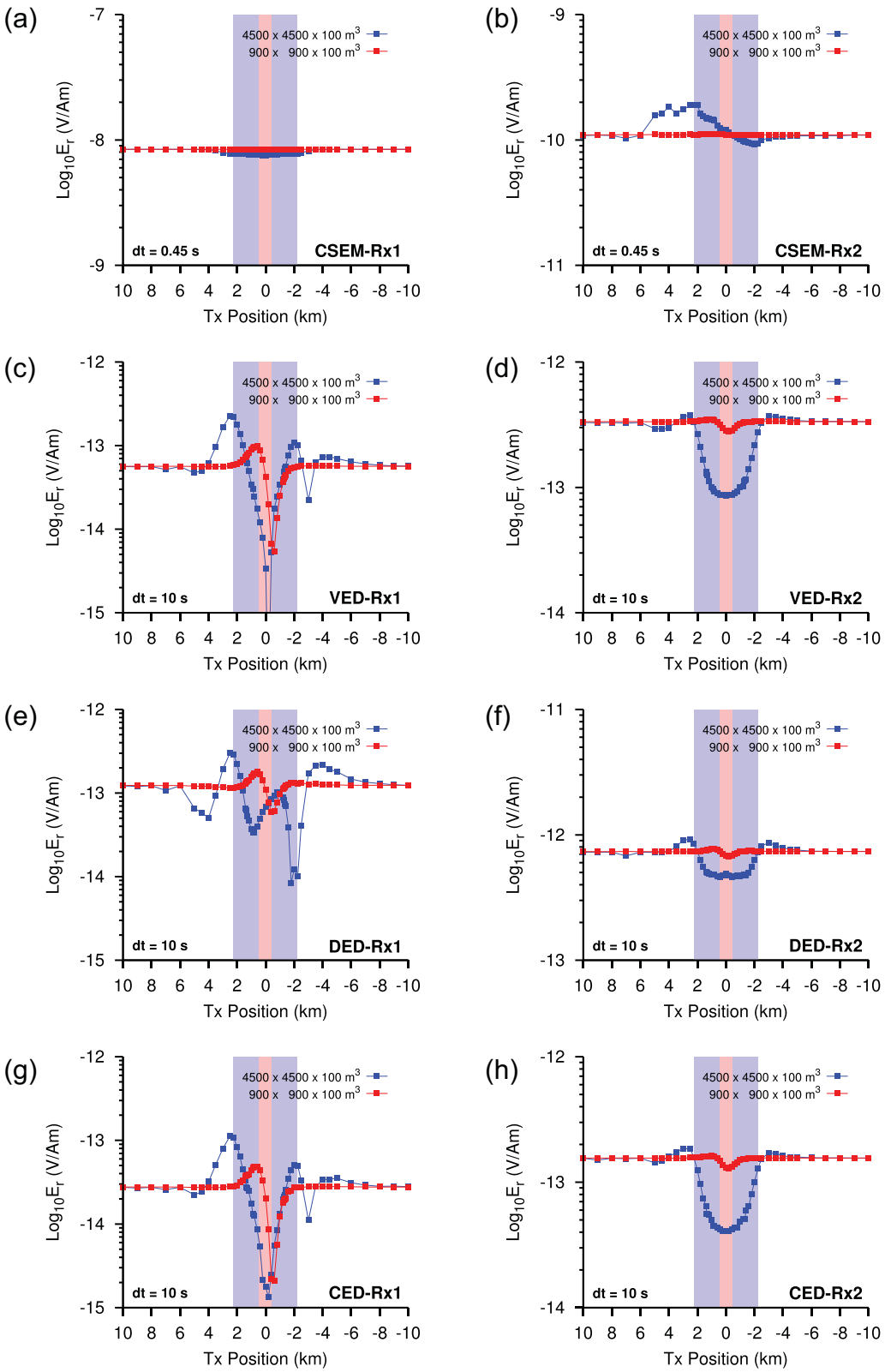

Figure 7. Profile plots of CSEM at time delays of $dt = 0.45$ s (a and b) and VED, DED and CED at time delays of $dt = 10$ s (c–h). The left column represents the short-offset configuration and the right column the long-offset configuration. The red line illustrates the response of the 900 m × 900 m body, the blue line the 4500 m × 4500 m body. The background colours represent the lateral dimensions of the resistive bodies.

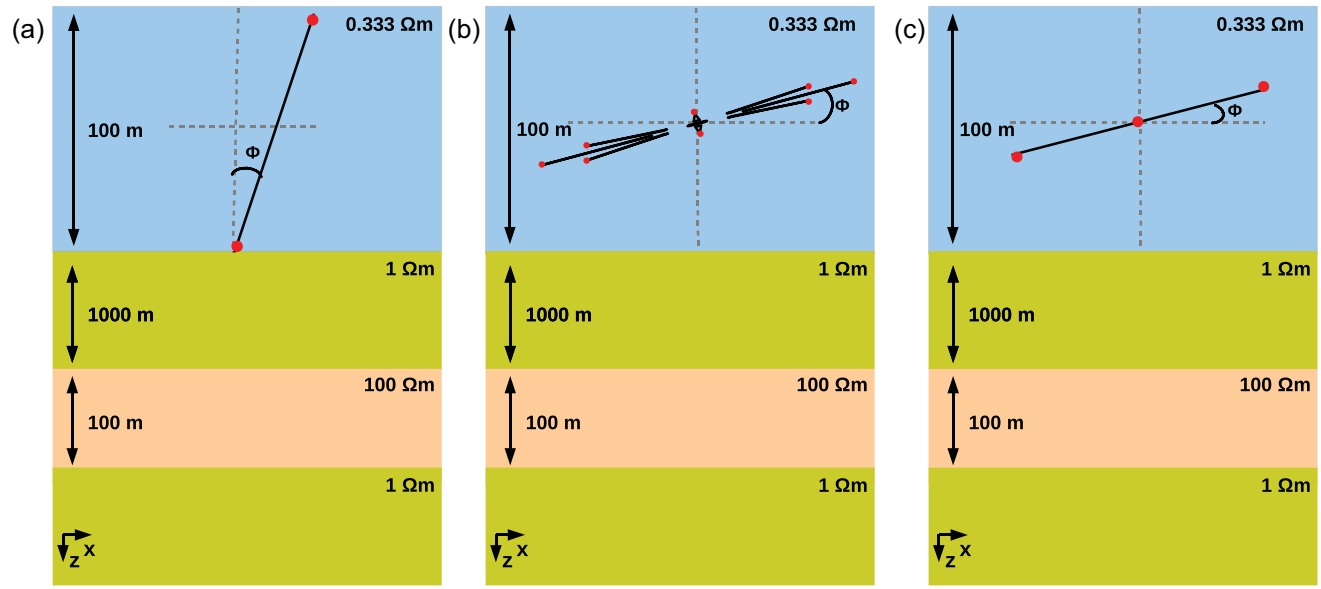

Figure 8. Schematic sketch of non-verticality modelling of VED (a), CED (b) and DED (c). The receivers are placed on the seafloor at an offset of 400 m. The transmitters are placed at the centre of the water column due to computational reason as explained in the text.

reservoir response but may lack the necessary SNR. The latter issue will need to be addressed prior to measuring as all three methods have a clear disadvantage compared to TD-CSEM. The enhanced lateral detectability of CED, VED and DED may still justify future application attempts.

The presented modelling studies have considered CED, DED, VED and even TD-CSEM applications in a rather idealistic manner. Up to now, the modelling study assumes a perfect transmitter antenna immune against geometrical errors. However, under real-world conditions where ocean currents, winds, etc. influence the measurement symmetry, this assumption is doubtful. Therefore, error studies are performed systematically investigating these influences on CED, DED, VED and TD-CSEM signals assuming symmetry distortions.

5 ERROR DUE TO NON-SYMMETRY OF THE TRANSMITTER

For land-based CED measurements, the issue of electrical symmetry (equal current amplitudes) within the eight transmitter arms is known and has been successfully solved through the development of a transmitter unit (Mogilatov & Balashov 1996; Helwig *et al.* 2010). By regulating the current amplitude in each arm individually, inhomogeneous coupling conditions were circumvented and the resulting error was minimized. In marine applications, the stability of the current regulation in the eight CED arms is less severe due to the homogeneous coupling in sea water. However, in comparison to land-based measurements, the geometrical symmetry of the transmitter caused by transmitter tilt or arm misplacement is more difficult to handle. The following modelling study will focus on the errors in transient behaviour caused by latter symmetry issues. The systematic errors of CED, DED and VED are evaluated and compared.

5.1 Non-verticality study

As shown in Fig. 8, let us first assume that the internal transmitter symmetry as a whole is maintained. For the CED transmitter displayed in Fig. 8(b), the eight arms are all in position with an angle of 45° between neighbouring arms. The transmitter as a whole is tilted by a certain angle Φ. Likewise, VED and DED transmitters displayed in Figs 8(a) and (c) are inclined by the same value. In fact, the non-verticality description originates from an imperfect VED. In this case, Φ describes the angle of inclination where $\Phi = 0^\circ$ represents an ideal, perfectly vertical transmitter. The underlying resistivity model is consistent to the 1-D modelling study in the prior section. The transmitter dipoles have a length of 100 m and the E_r receivers are located on the seafloor at an offset of 400 m.

The errors in transient behaviour are obtained by applying a superposition of transmitter components that arise in case of non-verticality. For DED and CED, this means an additional vertical transmitter component whereas VED has an additional horizontal component. Since we assume that a transmitter arm may not cross the seafloor interface, it was necessary to place the transmitter within the water column at an adequate distance from the seafloor. Consequently, the transmitter was placed in the centre of the water column to prevent one arm from crossing the seafloor interface even for large values of Φ. Generally, it would be preferable to model seafloor-based transmitters under the influence of bathymetry. However, this would require a multidimensional forward code, preferably using finite elements to discretize the model space. As mentioned, the modelling studies shown in Fig. 9 are done using a convenient 1-D forward code by superimposing transmitter components. Additional calculations were also performed for transmitters closer to the seafloor. In principle, these did not show significant differences to the results presented in this study.

The results of the non-verticality study for VED, CED and DED are displayed in Fig. 9. The absolute values of relative differences are displayed as a function of time and angle Φ in Figs 9(a), (c) and (e) for VED, CED and DED, respectively. Note that the colour bar for VED has a different range in comparison to CED/DED due to the greater error. Additionally, transients for selected values of Φ are shown in Figs 9(b), (d) and (f) for VED, CED and DED, respectively. We want to point out that, although the conventional VED systems as applied by Helwig *et al.* (2013) utilize an E_z receiver, where

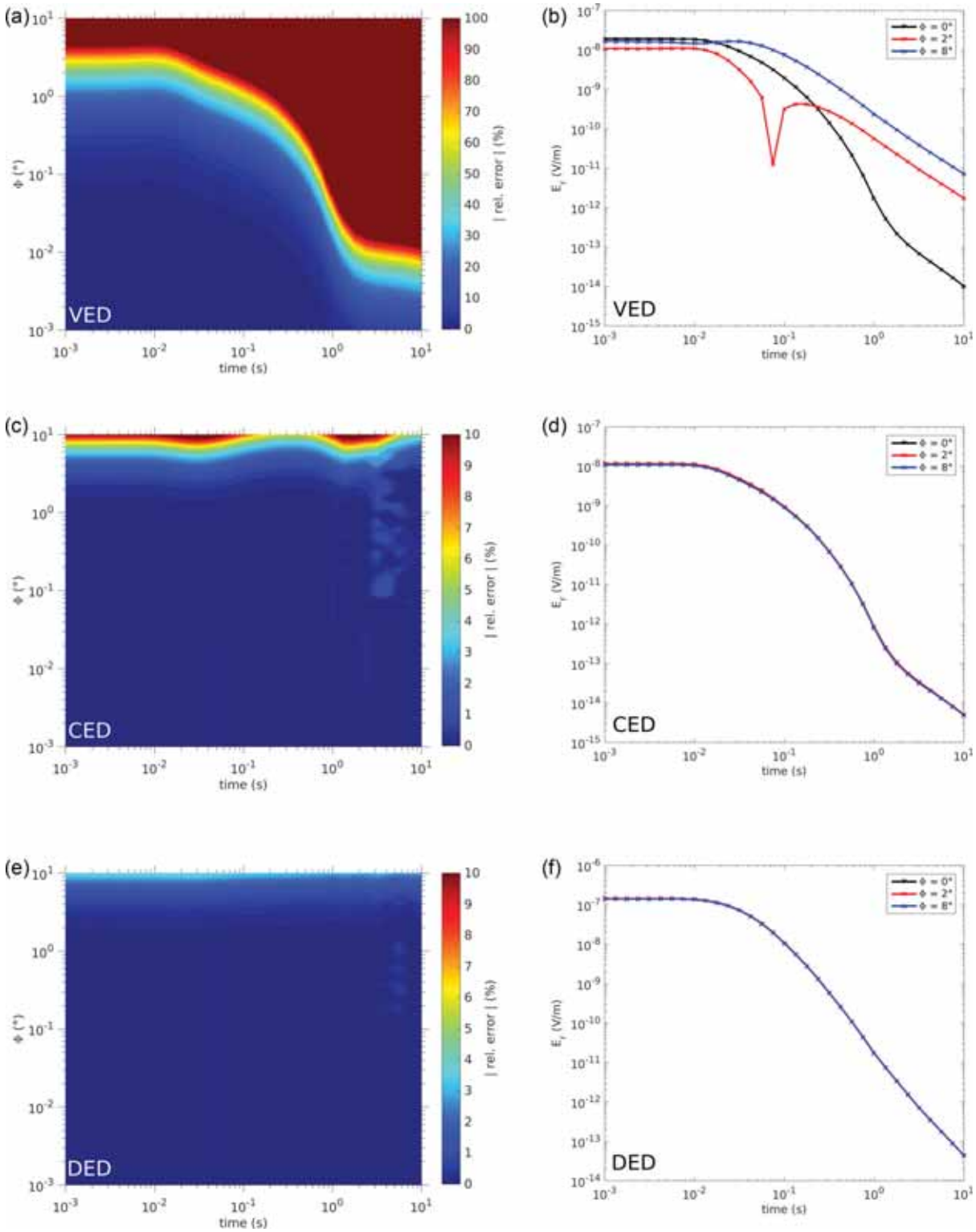

Figure 9. Non-verticality effect of VED (a and b), CED (c and d) and DED (e and f) for the configuration displayed in Fig. 8. The left column shows the absolute values of the relative differences plotted as a function of inclination and time, the right column shows transients at selected inclination angles of 0, 2 and 8 degrees. The colour bar of Fig. 9(a) is different from the ones of Figs 9(c) and (e).

the effect of non-verticality is less severe, we attempt to present a fair comparison between VED, CED and DED. Therefore, all modelling studies are performed with a radial electric field receiver. We relinquish the comparison to the TD-CSEM method as it is clear that an inclined HED will produce only a small geometric error (in form of a shift) for small angles and is not relevant for the purpose of this first study.

The results in Fig. 9 show that VED is particularly susceptible towards non-verticality, whereas DED and CED are rather insensitive towards this effect. To demonstrate the severe effect of this

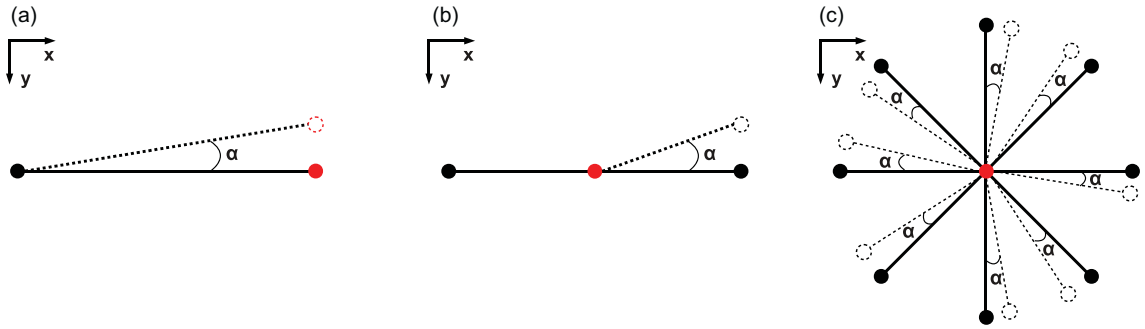

Figure 10. Geometrical error study investigating dipole movements of TD-CSEM (a), DED (b) and CED (c). The black circles represent electrodes with one polarity, the red circles the electrodes with the opposite polarity. The solid lines represent the ideal transmitter, whereas the dashed lines represent the altered transmitter. α is the angle between ideal and altered transmitter.

phenomenon on VED data, the investigated angles range from unrealistic values of $\Phi < 0.1^\circ$ to realistic values of $\Phi > 1^\circ$. For the investigated time range, the errors affect the intermediate to late times of the transient. This is associated with the slower signal decay of the parasitic HED component that arises if the VED transmitter deviates from perfect verticality. For a 100 m transmitter dipole, one would realistically expect Φ-values no smaller than 1° meaning that errors are produced exceeding 30 per cent even at very early times. In this case, the data may significantly falsify the interpretation of the subsurface resistivity structure.

In comparison to VED the signals of CED and DED are much less affected by non-verticality. For Φ-values exceeding 1°, errors in the transient behaviour are hardly notable throughout the entire time range. This is generally explained by the transmitter structure. An imperfect VED will generate a small but relevant HED signal that is especially prominent at late times. In contrast, the CED is assumed as a disc where the internal symmetry is held. Therefore, an inclination of the complete transmitter will solely produce a small additional vertical field component, which is considerably smaller in amplitude and, additionally, decays faster. Consequently, the error is solely geometric caused by the effective radius decrease due to inclination. This principle also applies to the DED transmitter.

It should also be mentioned that additional aspects that were not considered in this modelling study might have an effect on the results. The effect of non-verticality may increase/decrease depending on the offset and/or position of the receiver. Also, Goldman *et al.* (2015) show that an E_z receiver is less susceptible towards the effect non-verticality. The position of the transmitter within the water column may also affect the absolute error values but will generally not contradict the assertion of this study. If the internal symmetry of CED/DED is maintained, then a non-verticality effect is less prominent in comparison to VED.

5.2 Effect of asymmetric transmitter

The preceding non-verticality study assumed a perfect internal symmetry of the CED and DED transmitters, meaning the angle between the transmitter arms is 45° and 180°, respectively. In a realistic setup, this assumption can rarely be held, as the complex transmitter geometries are prone to minor errors. Errors in the range of several tenths of degrees are expected during the construction phase. Additionally, ocean currents at the seafloor may have an effect on the symmetry by producing small, but relevant arm movements. These effects are modeled in a static sense using the same 1-D resistivity model as above. As non-verticality of VED has the same effect as this symmetrical error, we confine to a comparison between CED, DED and TD-CSEM.

The transmitter geometry is consistent with the preceding studies. A dipole length of 100 m is applied with an E_r receiver at an offset of 400 m. Both transmitter and receiver are located on the seafloor. As illustrated in Fig. 10, moving one or more electrodes away from its ideal position in the xy-plane breaks the internal transmitter symmetry. The extent of alteration is described by angle α. For DED, only one of the outer electrodes is altered by α as a movement of both would maintain the symmetry in a similar sense as was investigated in the non-verticality study. In contrast, all outer electrodes of the CED transmitter are altered in opposite directions by α to simulate a realistic setting. An alteration of all electrodes in the same direction would maintain the transmitter symmetry.

Transients and relative errors of TD-CSEM, CED and DED for selected values of α are shown in Fig. 11. For small angles, TD-CSEM is hardly affected by the transmitter asymmetry. Even for $\alpha = 10^\circ$, the effect is negligible and typically lies in the error range of stacked data. This effect can be accounted for in the interpretation process. In comparison, the transients of CED and DED behave quite differently. The transients are shifted to a lower DC level at early times depending on the value of α. Additionally, the transient behaviour changes in comparison to the ideal geometry and, as a result, the errors explode at intermediate to late times. This especially applies if a sign reversal is caused in the transient due to geometrical distortions. Typically, DED tolerates small geometrical errors not exceeding several degrees whereas CED immediately punishes all deviations from a perfect symmetry. This issue makes an application of a CED system rather problematic in the marine environment as ocean currents may enforce small movements. In contrast, a successful DED application seems feasible but requires a precise positioning of the transmitter system. In general, TD-CSEM is easiest to implement, as geometric requirements are not as strict.

Although the errors caused by geometric asymmetry of a CED/DED may either increase or decrease depending on the underlying resistivity model, transmitter–receiver offset, dipole length, acquisition window, etc., they are in general agreement with the study shown in Fig. 11. We attempt to quantify the geometrical errors of CED and DED depending on the measurement setup in Fig. 12. The transmitter radius and offset is varied for different α-values while the background resistivity model stays consistent with the prior studies. For transmitter radius variations, the receiver is situated at an offset of four transmitter radii. The results are shown in form of an rms error expressed as the square root of the sum of squared relative differences divided by the number of data points. As the geometrical errors increase at late times for both CED and

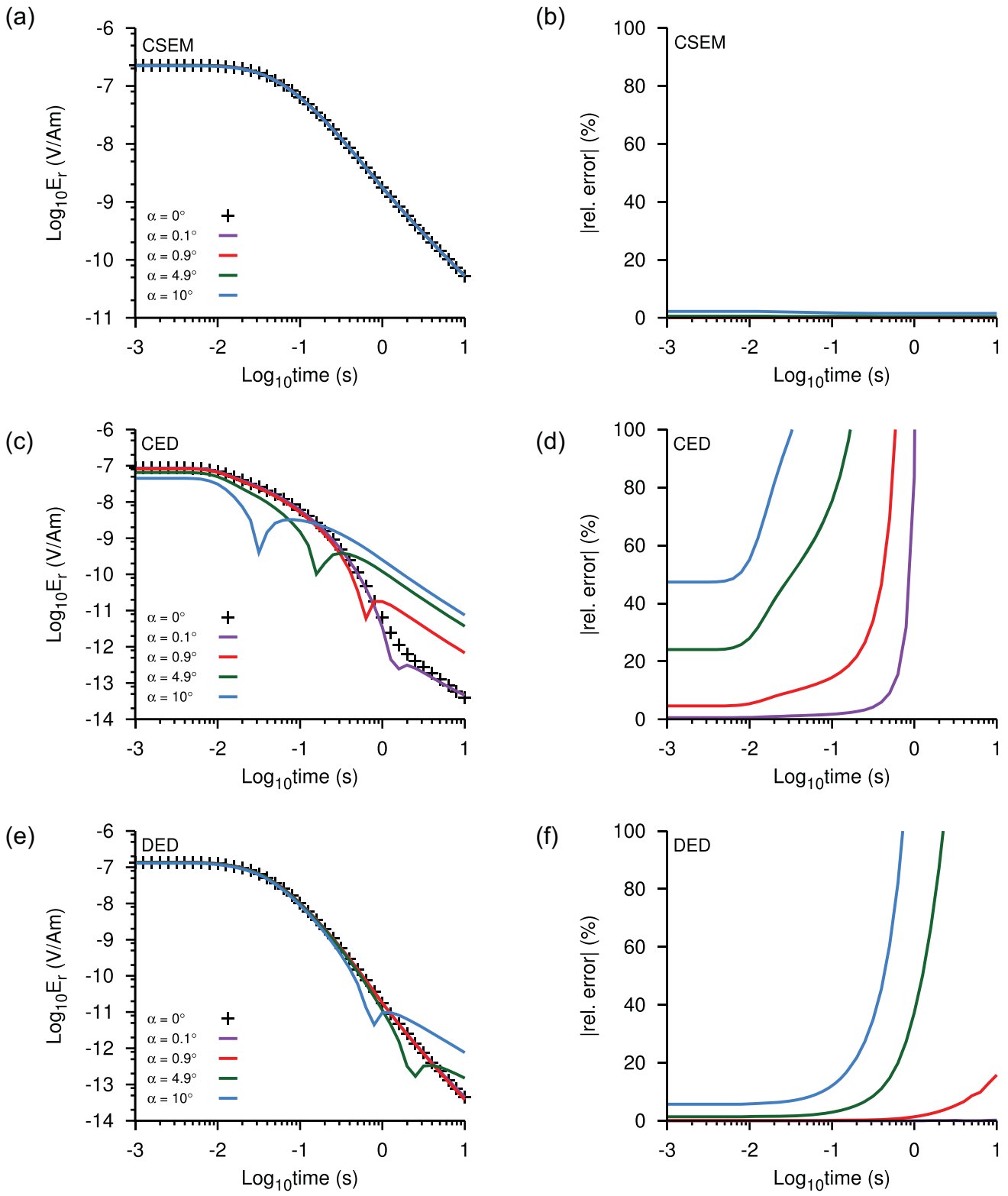

Figure 11. The transients for several values of α are displayed in the left column. The ideal setup of $\alpha = 0$ is displayed by markers whereas $\alpha \neq 0$ are displayed by coloured lines. In the right column, the relative differences between the obliterated and ideal transients are displayed.

DED, the relative difference at time delays of $dt = 10$ s is additionally displayed with white contour lines. It should be mentioned that all α-values smaller than 1° are practically unrealistic for actual field measurements. They simply demonstrate severity of the problem. Furthermore, under practical conditions, each transmitter arm will move by different α-values making the result even more unpredictable.

Small CED transmitters with radii smaller than 100 m are extremely susceptible to geometric errors. Even small values of $\alpha < 1e-2^\circ$ cause significant errors of up to 100 per cent, especially

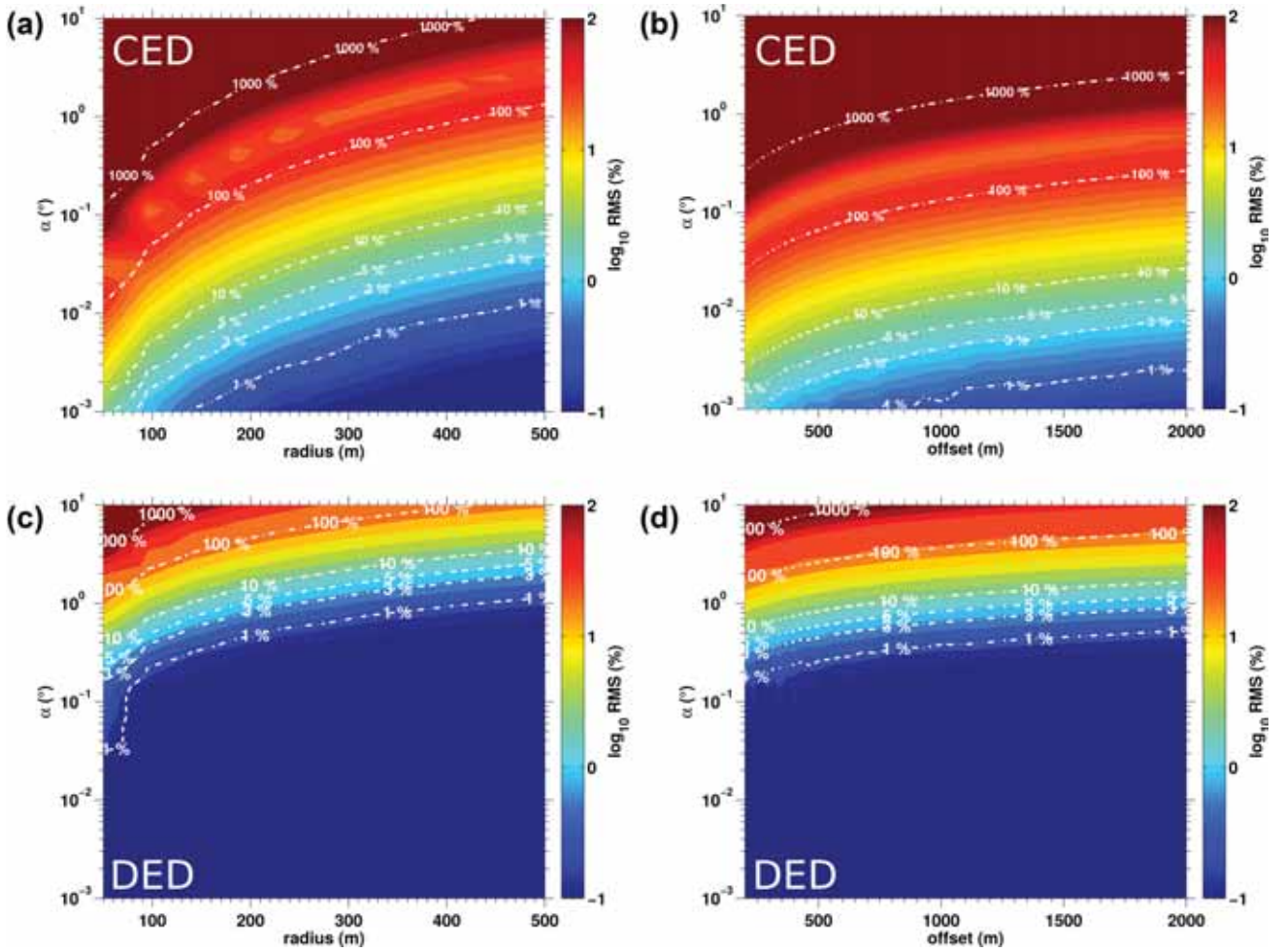

Figure 12. Geometrical error study for CED (top row) and DED (bottom row). The rms errors are plotted as a function of α and radius (left column)/offset (right column). The white contours represent the relative error at time delays of $t = 10$ s.

at late times. In comparison, the DED is less susceptible, especially if the transmitter radius is increased. Additionally increasing the offset further reduces the error. Hence, a trade-off between transmitter radius, offset, lateral resolution and SNR needs to be considered before executing actual measurements.

The results further show that a marine DED application may be more feasible compared to a marine CED application for two main reasons: (1) the transmitter is less susceptible to geometric errors and (2) increasing the transmitter radius and offset of a DED system is much more practical in comparison to CED, as everything is inline. Even a towed DED system seems quite feasible for future applications. In contrast, a marine CED transmitter is very costly to install, as the geometric requirements are very strict. A mobile measurement system is presently not imaginable. However, future marine CED applications may confine to reservoir monitoring using large, permanent transmitter systems with mobile receivers, similar to the land-based applications.

6 DISCUSSION

The comparative modelling studies show advantages/disadvantages of CED, DED, TD-CSEM and VED in a shallow-sea environment. The conventional TD-CSEM method is clearly the favourite in respect towards applicability and signal strength. The other methods have smaller signal amplitudes and are, additionally, susceptible towards geometrical errors. Increasing the induced current may account for the poor SNR while dipoles larger than 100 m will improve the effect of the geometrical errors. Yet, the SNR issue for marine CED and DED remains to be solved, as the amplitudes are significantly smaller in comparison to TD-CSEM. This is one of the major obstacles in future CED or DED applications. However, the latter methods show an exceptional sensitivity towards resistive bodies embedded in a conductive homogenous background environment. Consequently, an attempt to apply DED may still be justified despite the SNR issue.

The unimodal TM-mode methods CED and VED show high detectability characteristics towards resistive layers and are quite effective in delineating the lateral dimensions of 3-D resistive bodies as their signals are at maximum above the boundaries. However, an application of either method in shallow-sea environments seems rather doubtful at the present time. On the one hand is VED extremely susceptible towards the non-verticality effect. This is rather problematic for shallow-sea applications as the dipole has only a limited length and the ship positioning needs to be quite accurate. On the other hand is CED problematic due to the errors that occur if the transmitter symmetry is obliterated. This error can be reduced by applying large transmitter antennas, but is rather ineffective in a prospecting sense. Future monitoring projects with a permanently installed transmitter seem feasible.

As an alternative for shallow water EM applications, the novel DED method shows slightly improved detectability characteristics compared to TD-CSEM. Additionally, the method has similar features as CED/VED when delineating 3-D resistive bodies in both the short- and long-offset configuration. In comparison to CED/VED, the DED is less susceptible towards geometric errors and excites EM fields with amplitudes that are one order of magnitude larger. However, to serve as an alternative for TD-CSEM in shallow-sea applications, marine DED still needs a substantial development since its applicability has yet to be proven by actual field measurements. Furthermore, we have restricted the study towards detection of restive targets/layers and have not entirely addressed the issue of resolving electrical properties of the subsurface. Further development is, therefore, necessary to substantiate a DED application.

7 CONCLUSIONS

The novel marine CED method is still in the state of preliminary research and has yet to be applied in actual field measurements. The attempt to predict geometrical errors caused by an asymmetric transmitter exceeded 100 per cent relative error for realistic deviations of the ideal symmetry. As a consequence, the application of CED as suggested by Goldman *et al.* (2015) is rather questionable at the present time, even though its superior resolution capabilities makes its application desirable. As a compromise to the conventional TD-CSEM or VED methods, we propose to consider a further novel approach called DED. In a 1-D shallow marine environment, DED has similar detectability capabilities as TD-CSEM. The feasibility of DED has also not been tested yet, but modelling studies show that in comparison to CED, it is less susceptible to geometrical errors. However, an actual justification can only be given after a successful application of either DED or CED.

Clearly, the application of TD-CSEM is definitely the safest approach in obtaining data of good quality and may be sufficient in detecting resistive targets in a shallow marine setting. However, for small resistive 3-D targets, TD-CSEM has major disadvantages compared to VED/CED and even DED. An application of the latter may therefore be justified for these specific applications.

ACKNOWLEDGEMENTS

The authors would like to thank the anonymous reviewers and editor for their insights and comments regarding the manuscript. Their criticism substantially improved the scientific contents of the manuscript. The authors would like to acknowledge the German Research Foundation for the funding of the study. Also, the authors thank Dr. Carsten Scholl for providing the basic architecture of the 1-D inversion code in which the CED/DED forward solution was implemented.

REFERENCES

Barsukov, P.O. & Fainberg, E.B., 2014. The field of the vertical electric dipole immersed in the heterogeneous half-space, *Izv. Phys. Solid Earth,* **50,** 568–575.

Bubnov, V.P., Goldansky, V., Kashik, A.S., Mandelbaum, M.M., Rykhlinski, N.I. & Chemyak, V.V., 1984. Spatial differentiation in electric survey [in Russian], *Geol. Geophys.,* **6,** 106–111.

Chave, A.D & Cox, C.S., 1982. Controlled electromagnetic sources for measuring electrical-conductivity beneath the oceans. 1. Forward problem and model study, *J. geophys. Res.,* **87,** 5327–5338.

Chave, A.D., Constable, S. & Edwards, R.N., 1991. Electrical exploration methods for the seafloor, in *Electromagnetic Methods in Applied Geophysics,* Vol. 2, pp. 931–966, ed. Nabighian, M.N., Society of Exploration Geophysics.

Chen, J. & Alumbaugh, D., 2011. Three methods for mitigating airwaves in shallow water marine controlled-source electromagnetic data, *Geophysics,* **76**(2), F89–F99.

Connell, D. & Key, K., 2013. A numerical comparison of time and frequency-domain marine electromagnetic methods for hydrocarbon exploration in shallow water, *Geophys. Prospect.,* **61,** 187–199.

Constable, S., 2010. Ten years of marine CSEM for hydrocarbon exploration, *Geophysics,* **75,** A67–A81.

Davydycheva, S. & Rykhlinski, N., 2011. Focused-source electromagnetic survey versus standard CSEM: 3D modeling in complex geometries, *Geophysics,* **76**(1), F27–F41.

Druskin, V.L. & Knizhnerman, L.A., 1988. A spectral semi-discrete method for the numerical solution of three-dimensional non-stationary electrical prospecting problems, *Izv. Phys. Solid Earth,* **8,** 63–74.

Druskin, V.L. & Knizhnerman, L.A. 1994. Spectral approach to solving three-dimensional Maxwell's diffusion equations in the time and frequency domain, *Radio Sci.,* **29**(4), 937–953.

Edwards, N. 2005. Marine controlled source electromagnetics: principles methodologies, future commercial applications, *Surv. Geophys.,* **26,** 675–700.

Eidesmo, T., Ellingsrud, S., MacGregor, L.M., Constable, S., Sinha, S.A., Johansen, S., Kong, F.N. & Westerdahl, H., 2002. Sea Bed Logging (SBL), a new method for remote and direct identification of hydrocarbon filled layers in deepwater areas, *First Break,* **20,** 144–152.

Goldman, M., Mogilatov, V., Haroon, A., Levi, E. & Tezkan, B., 2015. Signal detectability of marine electromagnetic methods in the exploration of resistive targets, *Geophys. Prospect.,* **63,** 192–210.

Helwig, S.L., Mogilatov, V. & Balashov, B.P., 2010. The use of a circular electrical dipole source in hydrocarbon exploration, in *SEG Annual Meeting,* Houston, Texas, *Expanded Abstracts,* pp. 764–768.

Helwig, S.L., Kaffas, A.W., Holten, T., Frafjord, Ø. & Eide, K., 2013. Vertical dipole CSEM: technology advances from the Snøhvit field, *First Break,* **31,** 63–68.

Holten, T., Flekøy, E.G., Måløy, K.J. & Singer, B., 2009. Vertical source and receiver CSEM method in time domain, in *79th SEG Annual Meeting,* Houston, Texas, *Expanded Abstracts,* pp. 749–752.

Johansen, H.K. & Sørensen, K., 1979. Fast Hankel transforms, *Geophys. Prospect.,* **27,** 876–901.

Legeydo, P.Y., Mandelbaum, M.M. & Rykhlinski, N.I., 1990. Application of differentially adjusted electric exploration of the Nepa Dome [in Russian], *Sov. Geol. Geophys.,* **31,** 86–91.

Legeydo, P.Y., Mandelbaum, M.M. & Rykhlinski, N.I., 1997. Results of differential-normalized electrical prospecting in the Central part of the Nepa arch on the Siberian platform [in Russian], *Russ. Geol. Geophys.,* **38,** 1707–1713.

Mandelbaum, M.M., Ageenkkov, E.B., Legeydp, P.Y., Pesterev, P.Y. & Rykhlinski, N.I., 2002. Normalized-differential electrical measurements in hydrocarbon exploration: the state of the art and prospects for future, *Russ. Geol. Geophys.,* **43,** 1085–1143.

Mogilatov, V., 1992. A circular electric dipole as a new source in electric surveys, *Izv. Phys. Solid Earth,* **6,** 97–105.

Mogilatov, V., 1996. Excitation of a half-space by a radial current sheet source, *Pure appl. Geophys.,* **14**(7), 763–775.

Mogilatov, V. & Balashov, B., 1996. A new method of geoelectrical prospecting by vertical electric current soundings, *J. appl. Geophys.,* **36,** 31–41.

Scholl, C. & Edwards, N., 2007. Marine downhole to seafloor dipole-dipole electromagnetic methods and the resolution of resistive targets, *Geophysics,* **72,** P.WA39–P.WA49.

Singer, B. & Atramonova, S., 2013. Vertical electric source in transient marine CSEM: effect of 3D inhomogeneities on the late time response, *Geophysics,* **78,** P.E173–P.E188.

Swidinsky, A., Hölz, S. & Jegen, M., 2012. On mapping seafloor mineral deposits with central loop transient electromagnetics, *Geophysics,* **77**(3), E171–E184.

Veeken, P.C.H., Legeydo, P.J., Davidenko, Y.A., Kudryavceva, E.O., Ivanovm, S.A. & Chuvaev, A., 2009. Benefits of the induced polarization geoelectric method to hydrocarbon exploration, *Geophysics,* **74**(2), B47–B59.

Weidelt, P., 2007. Guided waves in marine CSEM, *Geophys. J. Int.,* **171,** 153–176.

Weiss, C., 2007. The fallacy of the "shallow-water problem" in marine CSEM exploration, *Geophysics,* **72**(6), A93–A97

APPENDIX: EXCITATION OF A RADIAL CURRENT SHEET

As shown in Fig. A1, the 1-D forward algorithm was developed for the ideal CED assuming a radial current sheet excitation. Additionally, the approximated CED, comprising of the superposition of eight HEDs arranged in a star-shaped pattern around a common centre (see Fig. 1), was also implemented in the forward algorithm. The DED works in a similar manner as the approximated CED but uses only two HEDs with a common central electrode (see Fig. 2). The aim is to obtain the electric and magnetic fields of a CED/DED with radius (b) at the seafloor.

The centre of the CED is located at point 0 of a cylindrical coordinate system (r, ϕ, z). The problem has an axial symmetry and only one magnetic component (B_Φ) satisfies the Helmholtz differential equation,

$$\partial_{rr} B_\phi + \frac{1}{r}\partial_r B_\phi - \frac{1}{r^2} B_\phi + \partial_{zz} B_\phi = \alpha^2 B_\phi \tag{A1}$$

where $\alpha^2 = i\omega\mu\sigma$ at all source-free points within zones of constant conductivity σ (S m^{-1}). This differential equation can be simplified by introducing a Hankel transform that relates any two arbitrary axial-symmetric functions $A(r, z)$ and $A(k, z)$ defined as:

$$A(r, z) = \int_0^\infty k\, A(k, z)\, J_1(kr)\, dk \tag{A2}$$

where J_1 is a Bessel function of first kind and first order. By applying the relation stated in eq. (A2) to B_Φ, and inserting it in eq. (A1), the Helmholtz equation simplifies to the following relation:

$$\partial_{zz} B_\phi(k, z) - \Theta_i^2 B_\phi(k, z) = 0 \tag{A3}$$

with $\Theta_i{}^2 = k^2 - i\omega\mu\sigma_i$.

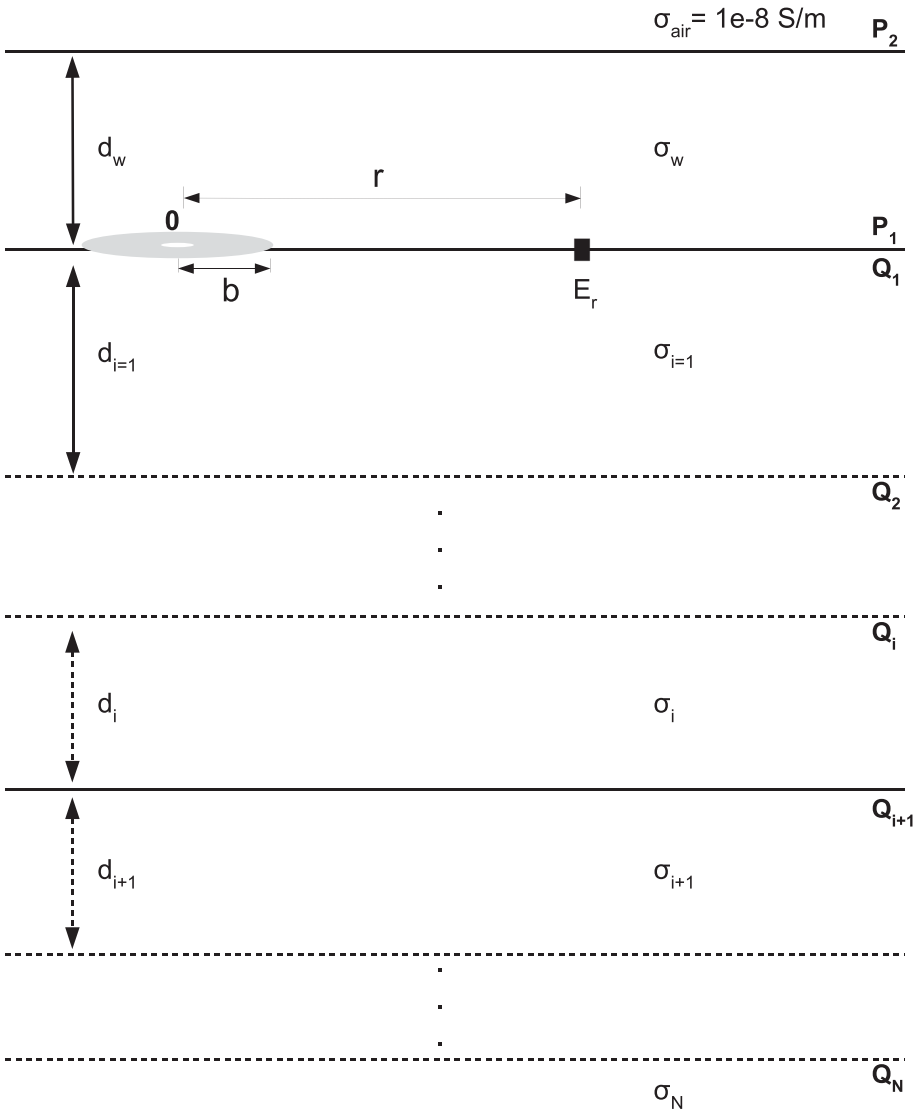

Figure A1. Sketch of a layered full-space model consisting of N-layers below the source and two layers above the source. The current excitation is caused by an ideal CED transmitter with inner radius $a \rightarrow 0$ and outer radius b.

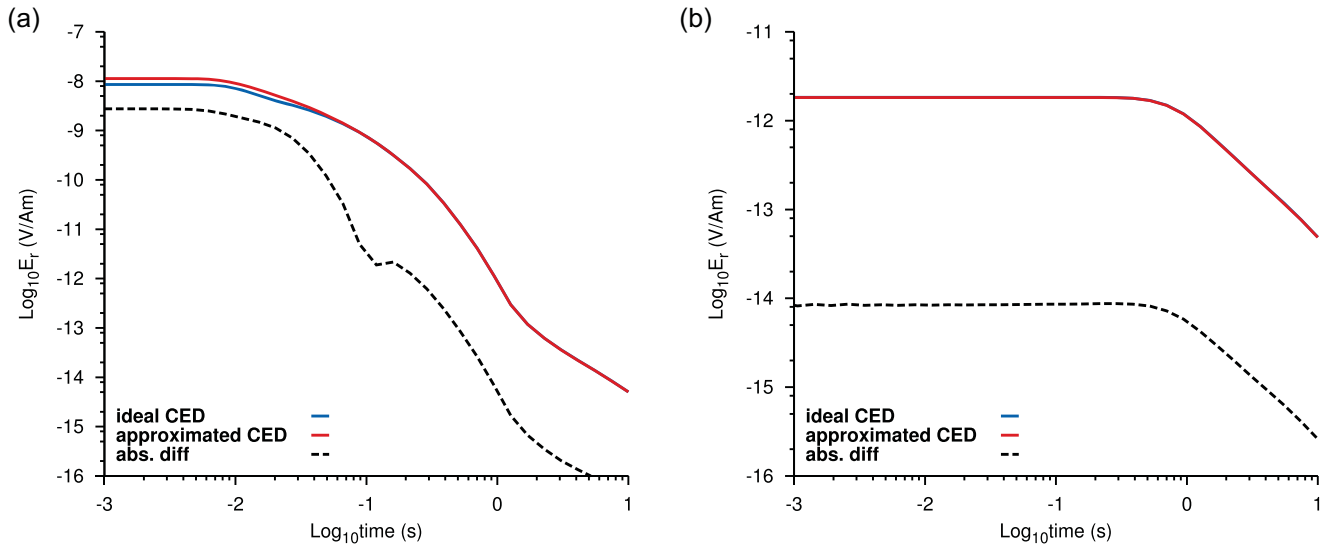

Figure A2. Comparison between transient of an ideal and approximated CED for the short-offset configuration (a) and long-offset configuration (b).

For a half-space consisting of N-layers beneath the transmitter (see Fig. A1), eq. (A3) describes a 1-D diffusion equation containing a resistivity $\rho_i = 1/\sigma_i$ (Ωm) with the solution in the form

$$B_{\phi_i} = C_i^+ \exp(-\Theta_i z) + C_i^- \exp(\Theta_i z) \tag{A4}$$

where C^+ and C^- are functions independent of z that are constrained by the boundary conditions. By eliminating C^+ and C^- and introducing the reciprocal impedance $Q_i = B_{\Phi,i}/\mu E_{r,I}$ (where E_r is derived from Ampere's law) and rearranging we obtain the upward recursion relationship from the bottom most terminating half-space to the source layer,

$$Q_i(k) = \frac{1}{\rho_i \Theta_i}\left[\frac{\rho_i \Theta_i Q_{i+1} + \tanh(\Theta_i d_i)}{\rho_i \Theta_i Q_{i+1}\tanh(\Theta_i d_i) + 1}\right], \tag{A5}$$

where Q_i and Q_{i+1} are the values of Q at the top of the ith and $(i+1)$th layer, respectively. For a given k, the value Q_1, directly beneath the source is recursively obtained through the relation stated in eq. (A5) starting in the lowest half-space with the starting condition,

$$Q_N = \frac{1}{\rho_N \Theta_N}. \tag{A6}$$

This procedure is repeated for the half-space above the source consisting of two layers (may be extended to M-layers) with the transfer function P defined as $P_j = -B_{\Phi,j}/\mu E_{r,j}$

$$P_1(k) = \frac{1}{\rho_1 \Theta_1}\left[\frac{\rho_1 \Theta_1 P_2 + \tanh(\Theta_1 d_1)}{\rho_1 \Theta_1 P_2 \tanh(\Theta_1 d_1) + 1}\right], \tag{A7}$$

where P_1 and P_2 are specific values of P at the bottom of the first and second layer above the source, respectively. The starting condition in the air layer above the source is defined as,

$$P_2 = P_{\text{Air}} = \frac{1}{\rho_{\text{Air}}\Theta_{\text{Air}}} \tag{A8}$$

where $\rho_{\text{Air}} = 10^8$ Ωm is the resistivity of the air layer. Outside of the source, the transfer functions, P and Q are continuous across the boundaries. By considering the boundary conditions at the source layer for a radial current sheet with density $j_r(r)$, the electrical field can be expressed as:

$$E_r(r,z) = \int_0^\infty J_1(kr)\cdot k \cdot S(k)\frac{P_1 Q_1}{P_1 + Q_1}dk \tag{A9}$$

where:

$$S(k) = \int_0^\infty j_r(r)\cdot r \cdot J_1(kr)\,dr\,. \tag{A10}$$

Within the radius of the source, we can now define $j_r(r)$ to be:

$$j_r(r) = \begin{cases} \frac{I_0}{2\pi r} & \text{for } a \le r \le b \\ 0 & \text{else} \end{cases} \tag{A11}$$

with current amplitude I_0. By inserting eq. (A11) into eq. (A10) we obtain the following expression for $S(k)$ (Mogilatov & Balashov 1996):

$$S(k) = \frac{I_0}{2\pi}\int_a^b J_1(kr)\,dr = \frac{I_0}{2\pi k}\left[J_0(ka) - J_0(kb)\right]. \tag{A12}$$

This expression describes a pair of grounded electrodes with inner radius a and outer radius b. We can now simplify this expression by assuming $a \to 0$ and therefore $J_0(ka) = 1$, meaning that we assume a point electrode at the centre of the radial current sheet. If we further assume that $b \ll r$ then $J_0(kb) \approx 1 - k^2b^2/4$. Therefore, the radial electric field at the source layer can now be computed according to Mogilatov & Balashov (1996):

$$E_r(r) = \frac{I_0 b^2}{8\pi}\int_0^\infty J_1(kr)\cdot k^2 \frac{P_1 Q_1}{P_1 + Q_1}dk \tag{A13}$$

where J_1 is the first kind Bessel-function of order 1, b is the radius of the CED transmitter and Q_1 and P_1 are the transfer functions just below/above the source layer calculated according to eqs (A5) and (A7), respectively. The observation in the time domain can be obtained by simply applying a fast Hankel transform of a half-integer order (Johansen & Sørensen 1979).

Field excitation of CED and DED using superposition of HED sources

The forward code also contains the solution of an approximated CED consisting of eight HEDs. This approach was implemented, as the solution is closer to the measured signal of field measurements. The theory for an HED field excitation is given in many academic literatures and will only be shown in respect towards a CED application here. As described, for example, by Edwards (2005), the

Laplace transform of the electrical field at distance r to the receiver is given by:

$$E(s) = \frac{j(s)}{2\pi}\left[F(s) + G(s)\right], \tag{A14}$$

where s is the Laplace variable, $j(s) = I\Delta l/s$ is the current dipole moment and $F(s)$ and $G(s)$ are the Laplace transforms of the TM mode and the TE mode, respectively. For an exact description of F and G for the inline and broadside configuration, refer to Edwards (2005). A superposition of two or more HED sources is simply performed by using eq. (A14) for each individual dipole followed by a simple addition. Hence, the electrical field at the receiver is obtained by:

$$\widetilde{E_r} = \sum_{i=1}^{n} E_i(s), \tag{A15}$$

where n describes the number of superimposed dipoles ($n = 2$ for DED and $n = 8$ for CED) and $E_i(s)$ is calculated according to eq. (A14). The main difficulty is to calculate the right offset and sign of current amplitude for each individual dipole.

A comparison of the algorithms is shown in Fig. A2 for the short- and long-offset configuration. The applied 1-D resistivity model is shown in Fig. 3 for a 100 m thick target formation. The offsets correspond to the ones used in the 1-D modelling study. The transient of the ideal and approximated CED is plotted with blue and red lines, respectively. The absolute difference of both transients is displayed with a blacked dashed line.

The early times of the short-offset configuration show minor differences. If this is caused by the TE mode of the approximated CED or by the approximation $J_0(kb) \approx 1 - k^2b^2/4$ is difficult to analyse. However, the solution of the ideal CED is in accordance with the solution of Mogilatov & Balashov (1996).